Letter

Spin-orbit coupling and interactions in quantum Hall states of graphene/WSe₂ heterobilayers

Dongying Wang ©, Mohammed Karaki, Nicholas Mazzucca ©, Haidong Tian, Guixin Cao ©, ChunNing Lau, Yuan-Ming Lu,* and Marc Bockrath†

Department of Physics, The Ohio State University, Columbus, Ohio 43210, USA

Kenji Watanabe 10

Research Center for Functional Materials, National Institute for Materials Science, 1-1 Namiki, Tsukuba 305-0044, Japan

Takashi Taniguchi D

International Center for Materials Nanoarchitectonics, National Institute for Materials Science, 1-1 Namiki, Tsukuba 305-0044, Japan



(Received 5 July 2021; revised 26 September 2021; accepted 27 October 2021; published 19 November 2021)

We use magnetotransport measurements to probe quantum Hall ground states in graphene/WSe₂ heterobilayers. Compared to pristine graphene, inter-Landau level (LL) gaps at half-filled quartets away from filling factor $\nu=0$ show significantly weaker dependence on the magnetic field B, while odd ν fillings show a stronger dependence. We interpret this behavior using a model incorporating Ising and Rashba spin-orbit coupling (SOC) along with Coulomb interactions within the self-consistent Hartree-Fock framework. A model fit yields Ising SOC in range $\sim 1-2$ meV, Rashba ~ 10 meV, and the in-plane dielectric constant ~ 12 , in agreement to previously found values. In the zeroth LL quartet, the $\nu=0$ gap as a function of magnetic field exhibits a plateau near 5 T, compared to $\sim 20-25$ T for pristine graphene. This behavior is in agreement with a model in which the SOC causes a phase transition from a canted antiferromagnetic state to a ferromagnetic state to occur at a much lower field. Our studies demonstrate how the interplay of SOC and electronic interactions affect graphene's electronic structure.

DOI: 10.1103/PhysRevB.104.L201301

Spin-orbit coupling (SOC) provides a promising route to controlling spin degrees of freedom in devices as well as realizing topological phases [1,2]. Graphene has emerged as a high mobility material with outstanding electronic properties. However, its intrinsic SOC is weak [3-6]. This has motivated many proposals and studies to induce SOC in graphene using proximity to other materials with stronger SOCs [7–24]. These include adatoms [7,8] as well as other two-dimensional (2D) materials such as transition metal dichalcogenides [9–18] (TMDs). Previous works have shown that coupling graphene to TMDs induces a SOC that can be detected from weak localization [11–16] and Shubnikov de Haas oscillations [13]. Moreover, coupling graphene to TMDs has the advantage of retaining graphenes high mobility. Recent work has shown that SOC can be measured from the quantum Hall effect (QHE) [17,18], where both valley Zeeman and Rashba SOC can be measured in the same device [17].

Because of electronic interactions, the QHE in mono- and few-layer graphene exhibits a rich phase diagram with various spin, valley, and layer orderings [25,26]. These symmetry-breaking interactions lift the degeneracy between quartets of Landau levels (LLs) in graphene [27,28]. As SOC splits the spin degeneracy and breaks inversion symmetry, it is expected to profoundly influence the many-body phases in graphene. However, a comprehensive study on graphene quantum Hall

effects, where both the SOC and interactions play important roles, has not been performed.

Here we report quantum Hall studies of monolayer graphene/monolayer tungsten diselenide (WSe2) structures encapsulated in hexagonal boron nitride (hBN). At low temperatures, within a perpendicular magnetic field B, we observe a Landau fan showing all integer quantum Hall states, which provides information of the spin and valley symmetry-breaking gaps. To investigate the LL structure with the influence of proximity-induced SOC, we use temperaturedependent transport measurements to determine the inter-LL gaps Δ_{ν} associated with the broken symmetry states in the QHE. All gaps increase with B with different characteristic slopes for electron and hole doping, deviating from the isolated graphene behavior [29]. A single-particle continuum model based on Dirac fermions with an out-of-plane Ising and in-plane Rashba SOCs is unable to account for the observed trends. We therefore include electron-electron interactions in a self-consistent Hartree-Fock approach. A good fit of the B-dependent gap behavior to the Hartree-Fock model is obtained, enabling us to extract the SOC parameters and the effective dielectric constant. In the zeroth LL, due to minimal screening of the Coulomb interaction at charge neutrality, the Hartree-Fock approach cannot capture the strong electronic interaction and fails to provide a satisfactory fit to the experimental data.

The longitudinal resistance as well as the measured gap vs. magnetic field both show a plateau near B = 5 T. This is consistent with a field-induced transition from a canted

^{*}lu.1435@osu.edu

[†]bockrath.31@osu.edu

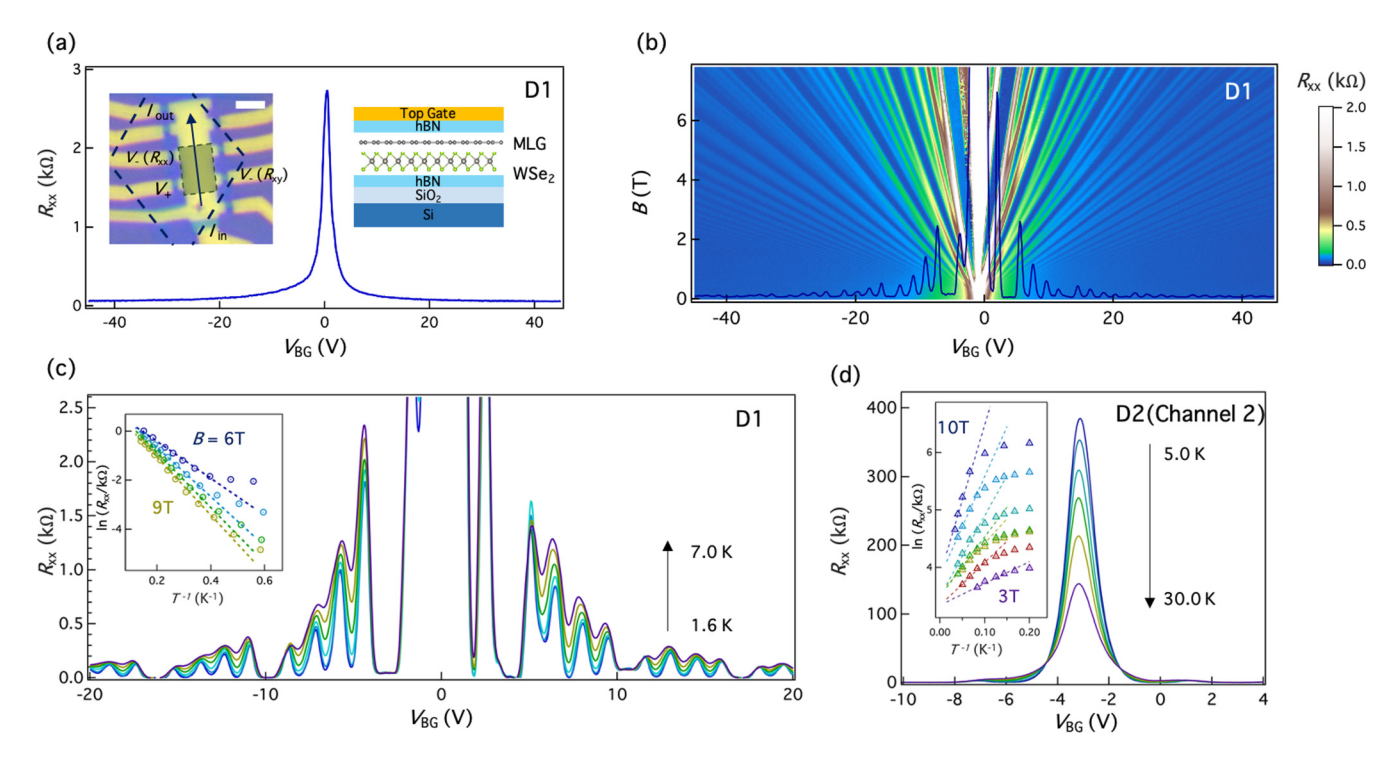


FIG. 1. All-integer quantum Hall effect in monolayer graphene on WSe₂. (a) Main panel: R_{xx} versus V_{BG} at T=1.5 K. Left inset: Optical image of an MLG/WSe₂ device. The dark blue dashed outline indicates the WSe₂ region before etching. Labels are included to indicate the current and voltage probes in use and the applied current direction is shown with the arrow. Green highlighted region is the measured area. Scale bar is 1.5 μ m. Right inset: Schematic diagram of the layer stack. (b) Landau Fan from a monolayer graphene on WSe₂ device. Splitting of the quartet LLs is visible above 3 T and quantum Hall gaps at all integer fillings become visible at 8 T (superimposed). (c) Temperature dependence of R_{xx} minima in symmetry broken quantum Hall states at B=9 T. Inset: Arrhenius plot for v=4 as a function of magnetic field. (d) Temperature dependence of the insulating state at v=0 at b=9 T. Inset: Arrhenius plot for v=0 as a function of magnetic field.

antiferromagnetic state to a ferromagnetic state [29,30], in which SOC drives this transition to a much lower magnetic field compared to that found in previous studies on isolated graphene [31–33]. A similar observation has been reported in monolayer graphene in proximity to yttrium iron garnet [34]. However, here we demonstrate that such behavior can occur in the absence of magnetic materials.

Our devices were fabricated using a dry transfer and stacking method [35]. Graphene and WSe₂ flakes were first exfoliated on SiO₂/Si substrates (285-nm-thick SiO₂) and then brought together and encapsulated in two hBN layers. After vacuum annealing and contact mode AFM cleaning [36], conventional electron beam lithography, and reactive ion etching techniques were employed to pattern multiterminal Hall bar geometry. A 5-nm/70-nm Cr/Au metal layer were then evaporated to make one-dimensional edge contacts [37]. The degenerately doped Si substrate acts as a back gate. The Fig. 1(a) left inset shows an optical image of a completed device as well as the measurement configuration. The right inset shows the layer stacking diagram. (We also employed a metal top gate to study the effects of displacement field, which shows no obvious influence, see Fig. 2(b) in the supplemental material [38].)

We obtained high-quality data from two separate monolayer graphene/monolayer WSe₂ devices, D1 and D2. To perform the measurements, completed devices were loaded into a variable-temperature flowing gas ⁴He cryostat. Transport measurements were performed at a base temperature T = 1.6 K using low-frequency lock-in techniques with a constant ac current of 50 nA. Within the whole measurement range, the Fermi level of WSe₂ is in its band gap [39]. All conducting signals we observed came from the graphene layer. In Fig. 1(a) (main panel), we show the longitudinal resistance R_{xx} as function of back gate voltage V_{BG} (applied to the Si layer) from a representative device. From the Drude model, we extract the field mobility to be 120 000 cm² V⁻¹ s⁻¹ at low temperature, indicating the high quality of our sample. With a perpendicular magnetic field B applied, a color plot of R_{xx} versus V_{BG} and B shows a Landau fan pattern [Fig. 1(b)], arising from the integer QHE of graphene. Consistent with the OHE in pristine monolayer graphene, the primary gaps occur at filling factors v = 4(n + 1/2), where n is the Landau level orbital index [40]. At those filling factors, the longitudinal resistance valleys show flat behavior near zero, while the transverse resistance shows well-developed plateaus at the appropriate quantized values as shown in the supplemental material [Fig. 2(a)] [38]. Fourfold degenerate LLs due to the spin and valley degeneracy can be split by perturbations such as electronic interactions and Zeeman splitting, as well as the proximity-induced SOC in our devices. Symmetry breaking gaps at half fillings of the nearly degenerate quartets (such as $\nu = \pm 4, 8, 12, \ldots$) begin to appear above B = 3 T. For B > 6 T, R_{xx} minima are visible at all integer QHE states. A line trace for R_{xx} as a function of V_{BG} at B=8 T is overlaid.

To determine the effect of the SOC on the LL spectrum, we determined the thermal activation gaps Δ_{ν} by measuring the

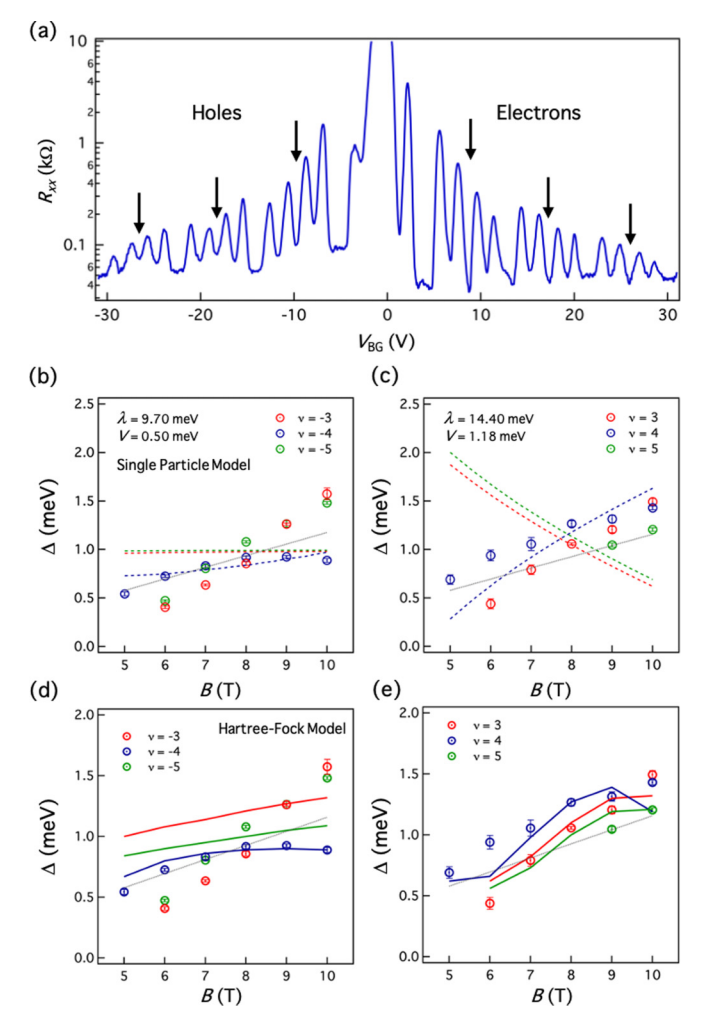


FIG. 2. Symmetry-broken quantum Hall states and theoretical fitting results. (a) R_{xx} vs. V_{BG} taken at B=8 T in a log scale. [(b) and (c)] Measured thermal activation gaps (open circles) and single-particle fitting results (dashed lines) for $\nu=-3,-4,-5$ and $\nu=3,4,5$. [(d) and (e)] Measured thermal activation gaps (open circles) for $\nu=\pm3,\pm4,\pm5$ as well as the corresponding Hartree-Fock fitting results (solid lines). Gray dotted lines represent the Zeeman splitting with g=2. Within each LL quartet, the fitting parameters for the even and odd filling factors are obtained separately. Data in this figure are all collected from sample D1.

temperature dependence of R_{xx} minima at a number of filling factors. These gaps are associated with the energy cost of the lowest-lying charged excitations of the ground state. The Δ_{ν} measurements enable us to extract quantitative information of the symmetry broken gaps in the presence of proximity-induced SOC. Examples of these measurements are shown in Figs. 1(c) and 1(d). The insets show Arrhenius plots for $\nu = 4$ [1(c) inset] and $\nu = 0$ [1(d) inset].

We begin our discussion with the evolution of symmetry broken gaps with the magnetic field. At very low perpendicular fields, R_{xx} minima are visible only at half quartet fillings, $\nu = \pm 4, 8, 12, \ldots$ Minima at quarter fillings of each quartet emerge and become deeper with increasing B. Figure 2(a) shows a log plot of R_{xx} versus V_{BG} at B=8 T. For electron doping, R_{xx} minima at half quartet fillings are much deeper

than minima at quarter fillings. The opposite holds true for hole doping for $n \ge 2$. Measured activation gaps vs. B for the first LL quartet are shown as open circles in Fig. 2(b) and 2(c). The B dependence of Δ_{ν} for all filling factors is similar, following an approximately linear scaling, except for $\nu = -4$. The hole side half-filled quartet LL gap, Δ_{-4} , grows more slowly with B, saturating eventually above 9 T. This trend becomes more pronounced for higher LL index ($\nu = -8, -12$, see Fig. S3 in the supplemental material [38]). In contrast, the half-filled quartet gaps in isolated graphene scale linearly with B with an enhanced g factor, resulting from exchange contributions [29]. Here we attribute the saturating behavior of these gaps observed in our samples to proximity induced SOCs.

To understand the impact of SOC on the LL structure and extracting the SOC parameters from the gaps, we start from a single-particle continuum Dirac model incorporating Rashba and Ising SOCs, parametrized by λ and V, respectively. Below is the noninteracting Dirac Hamiltonian considered in this work:

$$H = v_F(\tau_z \sigma_x \hat{\pi}_x + \sigma_y \hat{\pi}_y) + \frac{\lambda}{2} (\tau_z s_y \sigma_x - s_x \sigma_y) + V \tau_z s_z + b s_z, \tag{1}$$

where $v_F = 1 \times 10^6$ m/s is the Fermi velocity; and τ_i , s_i , and σ_i denote the Pauli matrices for the valley, spin, and sublattice degrees of freedom; and $\hat{\pi} = -i\hbar \nabla + eA$ is the momentum operator, where $b = g\mu B/2$ is the Zeeman splitting. This single-particle model preserves two U(1) symmetries generated by valley (τ_z) and sublattice-spin $(s_z\sigma_z)$ rotations. The antiunitary particle-hole symmetry, generated by $\mathcal{C} = \sigma_z \mathcal{K}$ where \mathcal{K} denotes complex conjugation, is explicitly broken by the Ising SOC $(\propto V)$ and Zeeman term $(\propto b)$. This symmetry breaking carries over when interactions are incorporated in the model, and it is manifested in the particle-hole asymmetry of activation gaps.

We have performed a fit for the measured gaps in each LL quartet. The results showed that this single-particle Hamiltonian does not capture more than one gap in each LL, as shown in Figs. 2(b) and 2(c). We therefore incorporate the effects of Coulomb interactions via a Hartree-Fock approximation [41], characterized by an in-plane dielectric constant ϵ .

Figures 2(d) and 2(e) show the calculated gaps plotted against B (solid lines) along with the data (open circles) for $\nu = -3$, -4, and -5 in the left panel and $\nu = 3$, 4, and 5 in the right panel. Both the characteristic value of the slope $d\Delta_{\nu}/dB$ for positive odd ν , as well as the saturating behavior at half quartet filling, are captured by the fits. On the hole side, the Hartree-Fock fits (e.g., the slope of $\Delta(B)$ curve) for odd ν do not match the data as well as the even ν fits. Since the small $|\vec{q}|$ intravalley Coulomb interaction between electrons of opposite spins dominates over the intervalley one, it screens better in the high-field ferromagnetic ground state at the even fillings than the odd fillings. Therefore it is less likely for the Hartree-Fock approximation to produce accurate results at an odd filling factor. The Rashba term, which contributes to the energy a term proportional to $1/\sqrt{B}$, can result in a saturation behavior of the gaps at large fields, as is observed at even, negative filling factors in the experimental data.

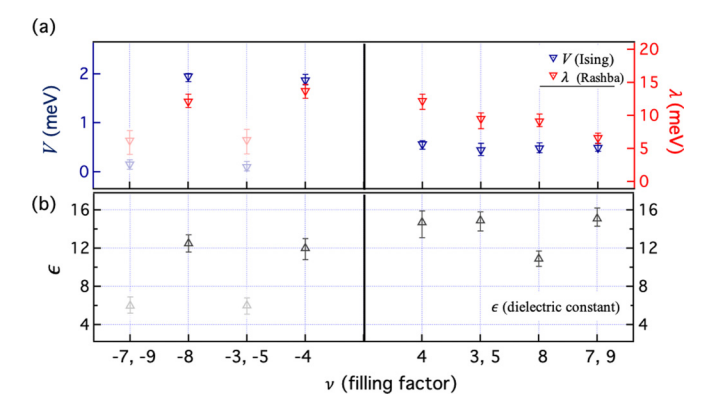


FIG. 3. Extracted SOC strength with Coulomb interactions incorporated in a self-consistent Hartree-Fock calculation. The Rashba and Ising SOC parameters (a) and the dielectric constant (b) from the Hartree-Fock fitting of the thermal activation gaps in each LL are considered separately. Hartree-Fock fitting results for negative odd filling shown in lighter colors are less accurate, likely due to less screened Coulomb interactions at odd fillings compared to even ones.

Figure 3 shows the obtained fit parameters for a number of different filling factors. These values appear consistent for the different quartets. We find an Ising SOC in range \sim 1–2 meV, a Rashba SOC \sim 12 meV, and a dielectric constant \sim 12, consistent with previous measurements [11–13,13–18]. It is worth mentioning that the SOC fitting parameters extracted from the data shows an electron-hole asymmetry, indicating the possible gate tunability of SOC strength. This is consistent with observed larger Ising SOC in valence bands of TMD compared to conduction bands [42–45]. Moreover, while monolayer hBNs dielectric constant is $\epsilon_{\parallel,1} \approx 6.8$, the dielectric constant of monolayer WSe₂ is $\epsilon_{\parallel,2} \approx 15.3$ [46], yielding a characteristic environmental dielectric constant $\bar{\epsilon}_{\parallel} = (\epsilon_{\parallel,1} + \epsilon_{\parallel,2})/2 \approx 11$ in reasonable agreement to the obtained value.

We now turn to the behavior of the zeroth LL quartet. A further notable feature of the experimental data is the plateau behavior of R_{xx} and Δ_0 near B=5 T. Figure 4(a) shows the longitudinal resistance R_{xx} as a function of B at charge neutrality. R_{xx} generally increases with B. An obvious slope decrease takes place around B = 5 T, as shown in the dashed box. To further look into the v = 0 quantum Hall state, we extract its thermal activation gap Δ_0 , according to the equation, $R_{xx} = R_0 e^{\Delta_0/2k_BT}$ [shown in Fig. 4(b)]. Consistent with the evolution of the longitudinal resistance, at B = 5 T, the gap size stops increasing and stabilizes around 1.2 meV and then increases again as the field continuously increasing. This observation deviates from previous results in isolated graphene, where an interaction-induced $\nu = 0$ gap shows a square root or sublinear dependence with magnetic field [29,47,48]. We attribute this behavior to a LL crossing induced by B, which is already visible in the single-particle model without Hartree-Fock corrections. As illustrated by Fig. 4(c), as the magnetic field increases, the Zeeman terms drives the spin up LLs

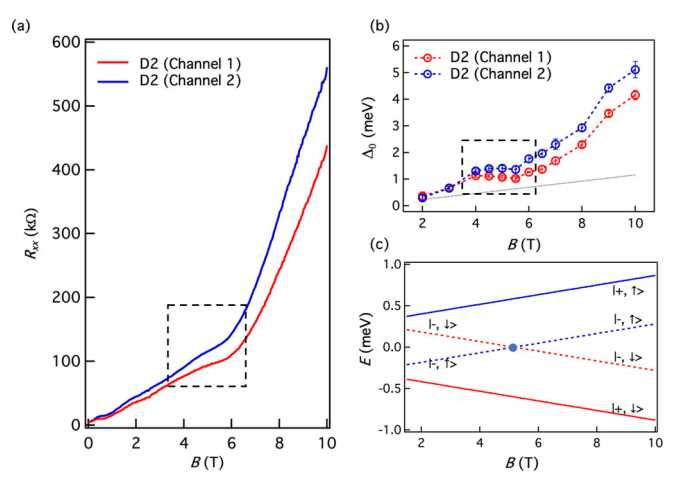


FIG. 4. Quantum Hall states near the charge neutral point. (a) Longitudinal resistance R_{xx} as a function of magnetic field B. (b) Measured thermal activation gap for $\nu = 0$. Gray dotted lines represent the Zeeman splitting with g = 2. (c) Simulated zero energy LL structure in single-particle model with V = 0.3 meV. Valley and spin information is noted for each LL branch. Data in this figure are collected from D2.

to decrease and the spin down LLs to increase in energy, resulting in a LL crossing of states with opposite spin in the K_- valley at $B \approx 5$ T. This indicates a phase transition from a canted antiferromagnetic state into a ferromagnetic state, leading to a kink in the transport gap Δ_0 as a function of magnetic field B as observed in Fig. 4(b). The critical B at which this transition occurs depends on the SOC strength in the single-particle model and can be modified by the Coulomb interaction.

In summary, we measured inter-Landau level activation gaps in WSe₂/graphene heterostructures via transport measurements versus perpendicular magnetic field and fit their behavior to a Dirac model including spin-orbit coupling in Coulomb interactions. We obtained values for the Ising and Rashba SOCs consistent with previous measurements. The behavior of the longitudinal resistivity in the zeroth Landau level shows a marked departure from the behavior found in pristine graphene. This can be understood as a transition from an canted antiferromagnetic to ferromagnetic a state that occurs at a low magnetic field because of the SOC. Future work, including parallel magnetic field measurements, is likely to yield additional insight into the interplay of SOC and interactions in 2D materials.

The experimental work is supported by NSF under Award No. DMR-2004801 (D.W. and M.B.). The theoretical work is supported by NSF under Award No. DMR-1653769 (M.K. and Y.-M.L.). Growth of hexagonal boron nitried crystals was supported by the Elemental Strategy Initiative conducted by the MEXT, Japan (Grant No. JPMXP0112101001) and JSPS KAKENHI (Grants No. 19H05790 and No. JP20H00354).

^[1] M. Z. Hasan and C. L. Kane, Rev. Mod. Phys. 82, 3045 (2010).

^[2] A. Manchon, H. C. Koo, J. Nitta, S. M. Frolov, and R. A. Duine, Nat. Mater. 14, 871 (2015).

- [3] J. C. Boettger and S. B. Trickey, Phys. Rev. B **75**, 121402(R) (2007)
- [4] S. Konschuh, M. Gmitra, D. Kochan, and J. Fabian, Phys. Rev. B 85, 115423 (2012).
- [5] R. van Gelderen and C. M. Smith, Phys. Rev. B 81, 125435 (2010).
- [6] J. Sichau, M. Prada, T. Anlauf, T. J. Lyon, B. Bosnjak, L. Tiemann, and R. H. Blick, Phys. Rev. Lett. 122, 046403 (2019).
- [7] J. Balakrishnan, G. Kok Wai Koon, M. Jaiswal, A. H. Castro Neto, and B. Özyilmaz, Nat. Phys. **9**, 284 (2013).
- [8] D. Marchenko, A. Varykhalov, M. R. Scholz, G. Bihlmayer, E. I. Rashba, A. Rybkin, A. M. Shikin, and O. Rader, Nat. Commun. 3, 1232 (2012).
- [9] A. Avsar, J. Y. Tan, T. Taychatanapat, J. Balakrishnan, G. K. W. Koon, Y. Yeo, J. Lahiri, A. Carvalho, A. S. Rodin, E. C. T. O'Farrell, G. Eda, A. H. Castro Neto, and B. Özyilmaz, Nat. Commun. 5, 4875 (2014).
- [10] L. A. Benítez, J. F. Sierra, W. Savero Torres, A. Arrighi, F. Bonell, M. V. Costache, and S. O. Valenzuela, Nat. Phys. 14, 303 (2018).
- [11] Z. Wang, D.-K. Ki, J. Y. Khoo, D. Mauro, H. Berger, L. S. Levitov, and A. F. Morpurgo, Phys. Rev. X 6, 041020 (2016).
- [12] Z. Wang, D. Ki, H. Chen, H. Berger, A. H. MacDonald, and A. F. Morpurgo, Nat. Commun. 6, 8339 (2015).
- [13] B. Yang, M.-F. Tu, J. Kim, Y. Wu, H. Wang, J. Alicea, R. Wu, M. Bockrath, and J. Shi, 2D Mater. 3, 031012 (2016).
- [14] B. Yang, M. Lohmann, D. Barroso, I. Liao, Z. Lin, Y. Liu, L. Bartels, K. Watanabe, T. Taniguchi, and J. Shi, Phys. Rev. B 96, 041409(R) (2017).
- [15] T. Wakamura, F. Reale, P. Palczynski, S. Guéron, C. Mattevi, and H. Bouchiat, Phys. Rev. Lett. 120, 106802 (2018).
- [16] S. Zihlmann, A. W. Cummings, J. H. Garcia, M. Kedves, K. Watanabe, T. Taniguchi, C. Schönenberger, and P. Makk, Phys. Rev. B 97, 075434 (2018).
- [17] D. Wang, S. Che, G. Cao, R. Lyu, K. Watanabe, T. Taniguchi, C. N. Lau, and M. Bockrath, Nano Lett. 19, 7028 (2019).
- [18] J. O. Island, X. Cui, C. Lewandowski, J. Y. Khoo, E. M. Spanton, H. Zhou, D. Rhodes, J. C. Hone, T. Taniguchi, K. Watanabe, L. S. Levitov, M. P. Zaletel, and A. F. Young, Spinorbit-driven band inversion in bilayer graphene by the van der Waals proximity effect, Nature 571, 85 (2019).
- [19] M. M. Asmar and S. E. Ulloa, Phys. Rev. B 91, 165407 (2015).
- [20] M. Gmitra and J. Fabian, Phys. Rev. B 92, 155403 (2015).
- [21] M. Gmitra and J. Fabian, Phys. Rev. Lett. 119, 146401 (2017).
- [22] J. Y. Khoo and L. Levitov, Phys. Rev. B 98, 115307 (2018).
- [23] J. Y. Khoo, A. F. Morpurgo, and L. Levitov, Nano Lett. 17, 7003 (2017).
- [24] A. De Martino, A. Hütten, and R. Egger, Phys. Rev. B 84, 155420 (2011).
- [25] M. O. Goerbig, R. Moessner, and B. Douçot, Phys. Rev. B **74**, 161407(R) (2006).
- [26] J. Alicea and M. P. Fisher, Solid State Commun. **143**, 504 (2007).

- [27] K. Nomura and A. H. MacDonald, Phys. Rev. Lett. 96, 256602 (2006).
- [28] Y. Zhang, Z. Jiang, J. P. Small, M. S. Purewal, Y.-W. Tan, M. Fazlollahi, J. D. Chudow, J. A. Jaszczak, H. L. Stormer, and P. Kim, Phys. Rev. Lett. 96, 136806 (2006).
- [29] A. F. Young, C. R. Dean, L. Wang, H. Ren, P. Cadden-Zimansky, K. Watanabe, T. Taniguchi, J. Hone, K. L. Shepard, and P. Kim, Nat. Phys. 8, 550 (2012).
- [30] M. Kharitonov, Phys. Rev. B 85, 155439 (2012).
- [31] P. Maher, C. R. Dean, A. F. Young, T. Taniguchi, K. Watanabe, K. L. Shepard, J. Hone, and P. Kim, Nat. Phys. 9, 154 (2013).
- [32] A. Young, J. Sanchez-Yamagishi, B. Hunt, S. Choi, K. Watanabe, T. Taniguchi, R. Ashoori, and P. Jarillo-Herrero, Nature (Lond.) 505, 528 (2014).
- [33] F. Chiappini, S. Wiedmann, K. Novoselov, A. Mishchenko, A. K. Geim, J. C. Maan, and U. Zeitler, Phys. Rev. B 92, 201412(R) (2015).
- [34] Y. Li, M. Amado, T. Hyart, G. P. Mazur, V. Risinggård, T. Wagner, L. McKenzie-Sell, G. Kimbell, J. Wunderlich, J. Linder, and J. W. A. Robinson, Phys. Rev. B 101, 241405(R) (2020).
- [35] C. R. Dean, A. F. Young, I. Meric, C. Lee, L. Wang, S. Sorgenfrei, K. Watanabe, T. Taniguchi, P. Kim, K. L. Shepard, and J. Hone, Nat. Nano. 5, 722 (2010).
- [36] M. R. Rosenberger, H.-J. Chuang, K. M. McCreary, A. T. Hanbicki, S. V. Sivaram, and B. T. Jonker, ACS Appl. Mater. Interfaces 10, 10379 (2018).
- [37] L. Wang, I. Meric, P. Y. Huang, Q. Gao, Y. Gao, H. Tran, T. Taniguchi, K. Watanabe, L. M. Campos, D. A. Muller, J. Guo, P. Kim, J. Hone, K. L. Shepard, and C. R. Dean, Science 342, 614 (2013).
- [38] See Supplemental Material at http://link.aps.org/supplemental/ 10.1103/PhysRevB.104.L201301 for additional experimental and theoretical results.
- [39] K. Kim, S. Larentis, B. Fallahazad, K. Lee, J. Xue, D. C. Dillen, C. M. Corbet, and E. Tutuc, ACS Nano 9, 4527 (2015).
- [40] Y. Zhang, Y.-W. Tan, H. L. Stormer, and P. Kim, Nature (Lond.) 438, 201 (2005).
- [41] X.-Z. Yan and C. S. Ting, Phys. Rev. B 95, 075107 (2017).
- [42] G.-B. Liu, W.-Y. Shan, Y. Yao, W. Yao, and D. Xiao, Phys. Rev. B 88, 085433 (2013).
- [43] K. Kośmider, J. W. González, and J. Fernández-Rossier, Phys. Rev. B 88, 245436 (2013).
- [44] H. Yuan, M. S. Bahramy, K. Morimoto, S. Wu, K. Nomura, B.-J. Yang, H. Shimotani, R. Suzuki, M. Toh, C. Kloc, et al., Nat. Phys. 9, 563 (2013).
- [45] H. Zeng, G.-B. Liu, J. Dai, Y. Yan, B. Zhu, R. He, L. Xie, S. Xu, X. Chen, W. Yao et al., Sci. Rep. 3, 1608 (2013).
- [46] A. Laturia, M. L. Van de Put, and W. G. Vandenberghe, npj 2D Mater. Appl. 2, 6 (2018).
- [47] D. A. Abanin, B. E. Feldman, A. Yacoby, and B. I. Halperin, Phys. Rev. B **88**, 115407 (2013).
- [48] B. Roy, M. P. Kennett, and S. Das Sarma, Phys. Rev. B **90**, 201409(R) (2014).